Open access • Journal Article • DOI:10.1088/0004-637X/722/2/1864

The ACS LCID Project. VI. The Star Formation History of The Tucana dSph and The Relative Ages of the Isolated dSph Galaxies — Source link

Matteo Monelli, Carme Gallart, Sebastian L. Hidalgo, Antonio Aparicio ...+11 more authors

Institutions: University of La Laguna, University of Tasmania, University of Minnesota, ETH Zurich ...+5 more institutions

Published on: 05 Oct 2010 - The Astrophysical Journal (IOP Publishing Ltd.)

Topics: Dwarf spheroidal galaxy, Star formation, Dwarf galaxy, Galaxy formation and evolution and Galaxy

The ACS LCID project. VI. The SFH of the Tucana dSph and the relative ages of the isolated dSph galaxies

Monelli, M ; Gallart, C ; Hidalgo, S L ; Aparicio, A ; Skillman, E D ; Cole, A A ; Weisz, D R ; Mayer, L ; Bernard, E J ; Cassisi, S ; Dolphin, A E ; Drozdovsky, I ; Stetson, P B

Abstract: We present a detailed study of the star formation history (SFH) of the Tucana dwarf spheroidal galaxy. High-quality, deep HST/ACS data, collected in the framework of the LCID project, allowed us to obtain the deepest color-magnitude diagram to date, reaching the old main-sequence turnoff (F814 29) with good photometric accuracy. Our analysis, based on three different SFH codes, shows that Tucana is an old and metal-poor stellar system, which experienced a strong initial burst of star formation at a very early epoch (sime13 Gyr ago) which lasted a maximum of 1 Gyr (sigma value). We are not able to unambiguously answer the question of whether most star formation in Tucana occurred before or after the end of the reionization era, and we analyze alternative scenarios that may explain the transformation of Tucana from a gas-rich galaxy into a dSph. Current measurements of its radial velocity do not preclude that Tucana may have crossed the inner regions of the Local Group (LG) once, and so gas stripping by ram pressure and tides due to a close interaction cannot be ruled out. A single pericenter passage would generate insufficient tidal heating to turn an originally disky dwarf into a true dSph; however, this possibility would be consistent with the observed residual rotation in Tucana. On the other hand, the high star formation rate measured at early times may have injected enough energy into the interstellar medium to blow out a significant fraction of the initial gas content. Gas that is heated but not blown out would also be more easily stripped via ram pressure. We compare the SFH inferred for Tucana with that of Cetus, the other isolated LG dSph galaxy in the LCID sample. We show that the formation time of the bulk of star formation in Cetus is clearly delayed with respect to that of Tucana. This reinforces the conclusion of Monelli et al. that Cetus formed the vast majority of its stars after the end of the reionization era implying, therefore, that small dwarf galaxies are not necessarily strongly affected by reionization, in agreement with many state-of-the-art cosmological models. Based on observations made with the NASA/ESA Hubble Space Telescope, obtained at the Space Telescope Science Institute, which is operated by the Association of Universities for Research in Astronomy, Inc., under NASA contract NAS5-26555. These observations are associated with program 10505.

DOI: https://doi.org/10.1088/0004-637X/722/2/1864

The SFH of the Tucana dSph and the relative ages of the isolated dSph galaxies. Astrophysical Journal Letters, 722(2):1864-1878.
DOI: https://doi.org/10.1088/0004-637X/722/2/1864

The Astrophysical Journal, 722:1864–1878, 2010 October 20 doi:10.1088/0004-637X/722/2/1864

THE ACS LCID PROJECT. VI. THE STAR FORMATION HISTORY OF THE TUCANA dSph AND THE RELATIVE AGES OF THE ISOLATED dSph GALAXIES*

M. Monelli[1,2], C. Gallart[1,2], S. L. Hidalgo[1,2], A. Aparicio[1,2], E. D. Skillman[3], A. A. Cole[4], D. R. Weisz[3], L. Mayer[5,6], E. J. Bernard[7], S. Cassisi[8], A. E. Dolphin[9], I. Drozdovsky[1,2,10], and P. B. Stetson[11]

[1] Instituto de Astrofísica de Canarias, La Laguna, Tenerife, Spain; ebernard@iac.es, monelli@iac.es, carme@iac.es, dio@iac.es, antapaj@iac.es, slhidalgo@iac.es
[2] Departamento de Astrofísica, Universidad de La Laguna, Tenerife, Spain
[3] Department of Astronomy, University of Minnesota, Minneapolis, MN 55455, USA; skillman@astro.umn.edu
[4] School of Mathematics & Physics, University of Tasmania, Hobart, Tasmania, Australia; andrew.cole@utas.edu.au
[5] Institut für Theoretische Physik, University of Zurich, Zürich, Switzerland; lucio@physik.unizh.ch
[6] Department of Physics, Institut für Astronomie, ETH Zürich, Zürich, Switzerland; lucio@phys.ethz.ch
[7] Institute for Astronomy, University of Edinburgh, Royal Observatory, Blackford Hill, Edinburgh EH9 3HJ, UK; ejb@roe.ac.uk
[8] INAF-Osservatorio Astronomico di Collurania, Teramo, Italy; cassisi@oa-teramo.inaf.it
[9] Raytheon, 1151 E. Hermans Road, Tucson, AZ 85706, USA
[10] Astronomical Institute, St. Petersburg State University, St. Petersburg, Russia
[11] Dominion Astrophysical Observatory, Herzberg Institute of Astrophysics, National Research Council, 5071 West Saanich Road, Victoria, British Columbia V9E 2E7, Canada; peter.stetson@nrc-cnrc.gc.ca

Received 2010 June 17; accepted 2010 August 27; published 2010 October 5

ABSTRACT

We present a detailed study of the star formation history (SFH) of the Tucana dwarf spheroidal galaxy. High-quality, deep *HST*/ACS data, collected in the framework of the LCID project, allowed us to obtain the deepest color–magnitude diagram to date, reaching the old main-sequence turnoff (F814 $\sim$ 29) with good photometric accuracy. Our analysis, based on three different SFH codes, shows that Tucana is an old and metal-poor stellar system, which experienced a strong initial burst of star formation at a very early epoch ($\simeq$13 Gyr ago) which lasted a maximum of 1 Gyr (sigma value). We are not able to unambiguously answer the question of whether most star formation in Tucana occurred before or after the end of the reionization era, and we analyze alternative scenarios that may explain the transformation of Tucana from a gas-rich galaxy into a dSph. Current measurements of its radial velocity do not preclude that Tucana may have crossed the inner regions of the Local Group (LG) once, and so gas stripping by ram pressure and tides due to a close interaction cannot be ruled out. A single pericenter passage would generate insufficient tidal heating to turn an originally disky dwarf into a true dSph; however, this possibility would be consistent with the observed residual rotation in Tucana. On the other hand, the high star formation rate measured at early times may have injected enough energy into the interstellar medium to blow out a significant fraction of the initial gas content. Gas that is heated but not blown out would also be more easily stripped via ram pressure. We compare the SFH inferred for Tucana with that of Cetus, the other isolated LG dSph galaxy in the LCID sample. We show that the formation time of the bulk of star formation in Cetus is clearly delayed with respect to that of Tucana. This reinforces the conclusion of Monelli et al. that Cetus formed the vast majority of its stars after the end of the reionization era implying, therefore, that small dwarf galaxies are not necessarily strongly affected by reionization, in agreement with many state-of-the-art cosmological models.

Key words: galaxies: evolution – galaxies: individual (Tucana dSph) – galaxies: photometry – Galaxy: stellar content – Local Group

1. INTRODUCTION

Nearby galaxies in the Local Group (LG) present a variety of different properties in terms of stellar populations, gas and metal content, morphological type, and mass. Understanding their differences and similarities and how these evolved with time can bring important insights into our knowledge of the formation and evolution of the LG, and of galaxies in general. The recovery of their full star formation history (SFH) plays a key role, being among the most powerful techniques to dig into the mechanisms that drove the evolution of stellar systems. Precise estimates of the epochs of star formation and their duration give direct information to compare the observed properties with predictions. This is particularly important for investigating the first stages of the life of galaxies, because the properties of the stellar populations during the first few gigayears can be used to trace the impact of a variety of different physical mechanisms. For example, a delay in the onset of the star formation, or a truncation of the SFH at a very old epoch can possibly be used to infer the role of cosmic reionization (e.g., Ikeuchi 1986; Rees 1986; Efstathiou 1992; Babul & Rees 1992; Chiba & Nath 1994; Quinn et al. 1996; Thoul & Weinberg 1996; Kepner et al. 1997; Barkana & Loeb 1999; Bullock et al. 2000; Tassis et al. 2003; Ricotti & Gnedin 2005; Gnedin & Kravtsov 2006; Okamoto & Frenk 2009; Sawala et al. 2010; Mayer 2010). On the other hand, an episodic rather than continuous SFH might trace interactions of dwarf galaxies in their orbit around bigger systems (Mayer et al. 2001) or a possible cycle related to changes in the interstellar medium linked to supernova (SN) explosions (Carraro et al. 2001; Stinson et al. 2007; Valcke et al.

* Based on observations made with the NASA/ESA *Hubble Space Telescope*, obtained at the Space Telescope Science Institute, which is operated by the Association of Universities for Research in Astronomy, Inc., under NASA contract NAS5-26555. These observations are associated with program 10505.

2008). What is crucial in these kinds of analyses is the capability to precisely and accurately recover how these systems formed stars as a function of time and to characterize their chemical evolution.

Within this general context, we selected a sample of isolated dwarf galaxy members of the LG, with the aim of deriving quantitative SFHs over their entire lifetime. The main objective of the LCID project (Local Cosmology from Isolated Dwarfs[12]) is to study the details of the evolution of nearby isolated galaxies, compare their properties and help constrain cosmological and galaxy formation and evolution models. A general description of the project and an overview of the results are presented in C. Gallart et al. (2011, in preparation). This paper is focused on the study of one the most isolated dSph galaxies in the LG, Tucana, with particular emphasis on the comparison of its properties with those of the Cetus dSph (Monelli et al. 2010b).

Understanding the currently isolated nature of Tucana and Cetus is challenging in the context of galaxy formation theories. Models have been proposed suggesting that dSph galaxies originate from small, initially gas-rich galaxies that lost their gas through tidal and ram-pressure interactions with their large host galaxies (see Mayer 2010 for a review). Before the LCID project, however, the existing observations of Cetus and Tucana did not allow us to draw definite conclusions on the exact nature of these galaxies, particularly regarding the question of how extended in time their SFHs were. In Monelli et al. (2010b) and this paper, we show that Cetus and Tucana are similar to the oldest Milky Way dSph satellites such as Draco, Ursa Minor, Sculptor, and Sextans, and therefore they do not follow the morphology–density relation observed among Milky Way dSph satellites (e.g., van den Bergh 1999). Their mere existence, therefore, imposes new constraints on dSph galaxy formation models.

The first mention of the Tucana dSph appears in the Southern Galaxy Catalogue published by Corwin et al. (1985), but it was later "rediscovered" by Lavery (1990). The first color–magnitude diagram (CMD) was presented in Lavery & Mighell (1992), based on Anglo-Australian 3.9 m V, I images. Tucana appeared as an elongated spheroid ($e = 0.5$) and was classified as a dE5. Although their photometry was quite shallow, Lavery & Mighell (1992) could give the first estimates of the distance ($(m - M) < 24.75$), metal content ([Fe/H] $= -1.9$), and luminosity ($M_V = -9.5$). Tucana was definitively recognized as a member of the LG, with the peculiarity of being the first isolated dSph, not linked with either the Milky Way or M31. Lavery & Mighell (1992) also inferred that Tucana is a predominantly old system, based on the lack of young bright blue objects.

All these preliminary findings were later substantially confirmed by deeper data. Castellani et al. (1996) presented V, I photometry reaching $V \sim 26$ mag, which allowed them to estimate the distance ($(m - M)_I = 24.72 \pm 0.20$) based on the tip of the red giant branch (RGB) and a mean metallicity of [Fe/H] $= -1.56$, obtained comparing the Tucana RGB with the ridge line of Galactic globular clusters (GCs) from Da Costa & Armandroff (1990). Interestingly enough, they found that the color width of the RGB was larger than expected on the basis of the photometric errors. They interpreted this as a signature of a "consistent spread" in the metallicity of the Tucana stars.

A different conclusion was reached by Saviane et al. (1996), who presented V, I data collected with the EFOSC camera mounted on the 2.2 m ESO telescope. A comparison with the same database from Da Costa & Armandroff (1990) yielded a mean metallicity [Fe/H] ~ -1.80 and "no convincing indication of an abundance spread." An interesting point raised by Saviane et al. (1996) concerns the absolute dimension of Tucana. Using an exponential profile, they estimated a core radius of 166 pc, similar to that of the small Milky Way and M31 satellites (Mateo 1998).

Another very interesting characteristic of Tucana is the strong horizontal branch morphology gradient first detected by Harbeck et al. (2001), together with a double peak in the color distribution of the RGB stars. Based on these two hints and the likely absence of intermediate-age stars (supported by the non-detection of C stars; Battinelli & Demers 2000), Harbeck et al. (2001) suggested that Tucana experienced a very fast self-enrichment. This possibility was strongly supported by Bernard et al. (2008) on the basis of the properties of a sample of ∼400 RR Lyrae stars. They detected two different sub-populations of RR Lyraes having distinct spatial distributions and different mean luminosities, and following two period–amplitude relations with different slopes. This supports a scenario with two different sub-populations older than 10 Gyr, the more centrally concentrated one being slightly younger and slightly more metal-rich than the other.

The paper is organized as follows. Section 2 summarizes the observations and data reduction strategy. In Section 3, we present the CMD, while the derivation of the SFH is extensively discussed in Section 4. In Section 5, we compare the properties of the two isolated dSphs, Cetus and Tucana. Discussion and conclusions are presented in Sections 6 and 7.

2. OBSERVATIONS AND DATA REDUCTION

The data presented in this paper were collected with the ACS camera aboard the *Hubble Space Telescope* (*HST*; Ford et al. 1998), as part of the project *The onset of star formation in the universe: constraints from nearby isolated dwarf galaxies* (PID 10505, PI: C. Gallart).

The 32 orbits allocated to Tucana were executed between April 25 and 30, 2006. The observations were split into visits, each of them including two orbits. One F475W image and one F814W image were collected during each orbit, with exposure times slightly different among the two orbits of the same visit: 1070 s and 957 s in the first orbit; 1090 s and 979 s in the second one. Summarizing, the total observing time on Tucana was 34,560 s in F475W and 30,976 s in F814W. Note that, despite the fact that Tucana is the most distant galaxy in the LCID sample, the exposure times adopted are the shortest. This choice was forced due to the constraints imposed by the South Atlantic Anomaly.

The pointing ($\alpha = 22^{\rm h}41^{\rm m}48\overset{\rm s}{.}43$, $\delta = -64^\circ25'15\overset{''}{.}7$) was centered on the galaxy. Figure 1 shows a drizzled, stacked image. The parallel WFPC2 field already presented in Bernard et al. (2009) was intended to sample the halo of Tucana along its major axis, at the position ($22^{\rm h}40^{\rm m}52\overset{\rm s}{.}92$, $-64^\circ24'28\overset{''}{.}9$). The CMD of this field, located 6′ from the Tucana center, does not show any convincing evidence that stars of Tucana are still present at this distance, since no RR Lyrae stars were detected.

2.1. Data Reduction

The details of the data reduction strategy, common to all the LCID galaxies, have been presented in Monelli et al. (2010b), so here we just recall the main points. We performed

[12] http://www.iac.es/project/LCID

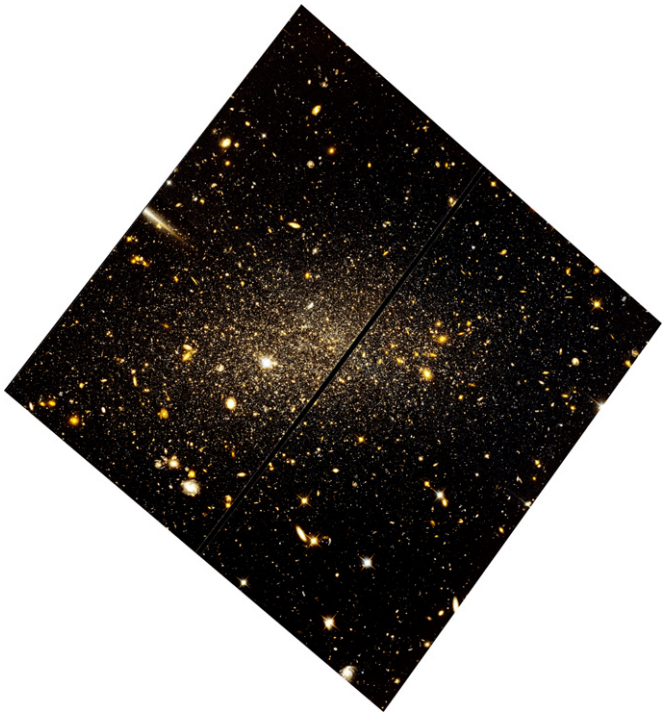

Figure 1. Stacked, drizzled color image of the Tucana field. North is up and east is left. The field of view is $\sim 3\farcm4 \times \sim 3\farcm4$. The image shows a clear gradient in the number of stars when moving from the center to the outskirts. A sizable number of background galaxies are visible as well.

two parallel and independent photometric reductions, using the DAOPHOT/ALLFRAME (Stetson 1994) and DOLPHOT packages (Dolphin 2000b). We applied both codes to the original _FLT images, working on the two chips separately. In the case of DAOPHOT, we modeled individual PSFs for each frame, using bright and isolated stars in the field. Typically, 400 stars and a Moffat function with index $\beta = 1.5$ were used.

The DOLPHOT code was applied using the ACS module and following the recommended photometry recipe provided in the manual for version 1.0.3.

Individual photometry catalogs for each frame were calibrated. We applied the calibration provided by Sirianni et al. (2005) identically to both sets of photometry. The final CMD is presented in Figure 2 and discussed in Section 3.

2.2. Completeness Tests

The completeness tests were performed by adding synthetic stars to the individual images and repeating the photometric analysis identically as for the real data.

In the case of the DAOPHOT photometry, the list of injected stars was created following the prescriptions introduced by Gallart et al. (1996), using a synthetic CMD created with IAC-star (Aparicio & Gallart 2004). This was built adopting a constant star formation rate between 0 and 15 Gyr and a metallicity distribution following a flat distribution in the range $0.0001 < Z < 0.005$. Approximately, 1,500,000 stars were simulated in each of the two chips, in iterations of ∼50,000 stars.

In the case of DOLPHOT, we followed the method described in Holtzman et al. (2006), simulating one star at a time and covering the range $-1\,\mathrm{mag} < M_{\mathrm{F475W}} - M_{\mathrm{814W}} < 5$ mag, $-7\,\mathrm{mag} < M_{\mathrm{F475W}} < 8$ mag. The density of injected stars is higher in the color–magnitude range where most of the observed stars are found. A total of 140,000 stars were simulated. We found that, at the level of the TO, the completeness is of the order of 80%.

2.3. Comparison of the Two Photometry Sets

We detect a small zero-point offset for the brightest stars in the m_{F475W} ($m_{\mathrm{F475W,DAO}} - m_{\mathrm{F475W,DOL}} = +0.019$ mag, for $m_{\mathrm{F475W}} < 25$) and in the m_{F814W} ($m_{\mathrm{F814W,DAO}} - m_{\mathrm{F814W,DOL}} = -0.008$ mag, for $m_{\mathrm{F814W}} < 24$) bands, and a trend as a function of magnitude. As already noticed in the case of Cetus (Monelli et al. 2010b), moving toward fainter magnitudes, DAOPHOT tends to measure stars slightly fainter. However, since the trend with magnitude is similar in the two bands, the color difference shows a small residual zero point (∼0.032 mag), but no dependence on the magnitude. As already noticed in the case of Cetus (Monelli et al. 2010b) and LGS 3 (Hidalgo et al. 2010), and discussed in Holtzman et al. (2006) in the case of the WFPC2, small differences in the photometry are expected when using different packages. Most importantly, we will show in Section 4.5 that the impact of the differences in the photometry on the derived SFH is negligible.

3. THE CMD

Figure 2, left panel, presents the final CMD for Tucana from the DAOPHOT photometry, calibrated to the VEGAMAG system and shifted to the absolute plane. The right panel shows the CMD of Cetus (Monelli et al. 2010b). The comparison of the two CMDs shows striking similarities in the different evolutionary features. An in-depth comparison of the CMDs and the properties of these two galaxies are presented in Section 5.

The Tucana CMD presented here is the deepest obtained for this galaxy to date. It spans more than ∼8 mag, from the tip of the RGB down to ≈1.5 mag below the oldest main-sequence (MS) turn-off (TO), or $M_{\mathrm{F814W}} \sim 4$. The absence of a blue young MS and the morphology of the old MSTO, at $M_{\mathrm{F814W}} \sim 2.5$ mag, are typical features of an old stellar system, with no strong recent or intermediate-age star formation. In agreement with what is commonly found in stellar systems, the plume of relatively faint objects appearing at $1.5 < M_{\mathrm{F814W}} < 3$, $0 < (M_{\mathrm{F475W}} - M_{\mathrm{F814W}}) < 0.5$ is most likely a population of blue stragglers. The possibility of some residual star formation occurring in the last 3–4 Gyr is discussed in Section 4.5. The RGB appears as a dominant feature, between $-4\,\mathrm{mag} < M_{\mathrm{F814W}} < 2$ mag. The width of the RGB suggests a limited spread in metallicity. The two over-densities located along the RGB at $M_{\mathrm{F814W}} \sim -0.9, -0.7$ and $M_{\mathrm{F475W}} - M_{\mathrm{F814W}} \sim +1.4$ and highlighted by two arrows are the RGB bumps (see Monelli et al. 2010a for a detailed study of the RGB bump feature in several LCID galaxies). The other clear over-density at $M_{\mathrm{F814W}} \sim -0.8$ and $M_{\mathrm{F475W}} - M_{\mathrm{F814W}} \sim 1.2$, and joining the RGB from the blue side, can be identified with the AGB bump and the subsequent AGB.

The Tucana HB, as previously noted by Harbeck et al. (2001), shows a complex morphology, which can be appreciated in detail in the present, much deeper data. It is well populated from the red to the blue side, to $M_{\mathrm{F475W}} - M_{\mathrm{F814W}} \sim 0$. A few bluer and fainter objects seem to continue the HB sequence, but they merge with the BS candidates and it is not possible to draw firm conclusions on their nature on the basis of the present data. A possible scenario to explain the strong blue component of the Tucana HB is that this feature is populated by a helium-enriched population. Helium-rich stars have been

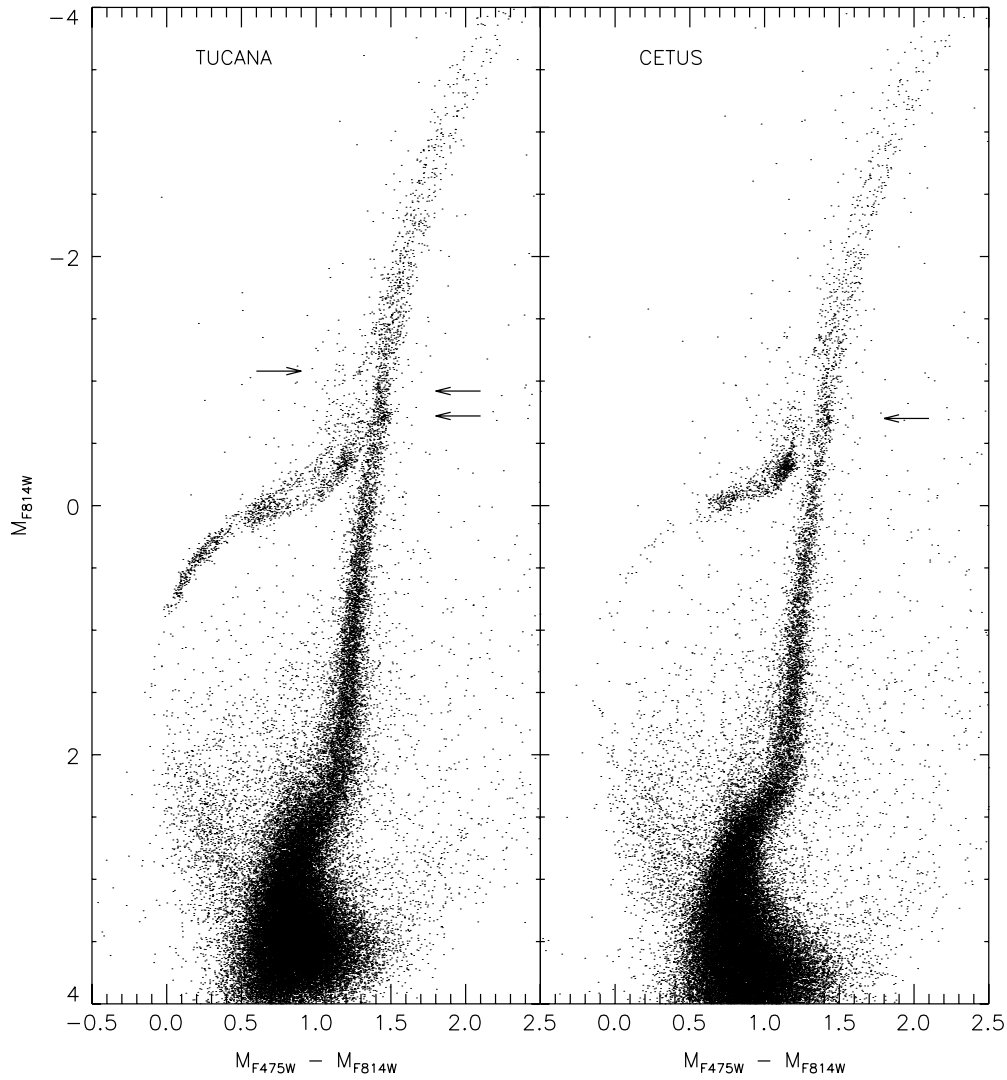

Figure 2. CMD of Tucana and Cetus obtained with DAOPHOT. Note that the color of the bluest HB stars is similar in both galaxies, but the number of blue HB stars is significantly higher in Tucana than in Cetus. The RGB bumps are also obvious features in both galaxies as indicated by the arrows on the right side of the RGBs. The arrow on the left side of the Tucana RGB mark the AGB clump (Monelli et al. 2010a).

invoked to explain the properties of the most massive Galactic GCs which have been proved to host more than one population (Piotto et al. 2005; Caloi & D'Antona 2005; Milone et al. 2008, 2010). The effect of the helium enrichment is to produce, at fixed age and for $M_{F475W} - M_{F814W} > -0.2$, a bluer and brighter HB. Figure 3 shows the Tucana CMD with selected zero-age horizontal branches (ZAHBs) from the BaSTI database superimposed, for metallicity $Z = 0.0001$, 0.0003, 0.0006 and $Y = 0.245$, 0.30, 0.35. The figure shows that the HB is nicely bracketed by the canonical helium ZAHBs and a metallicity in the range 0.0003–0.001. Note that this is in excellent agreement with the results of the SFH, suggesting a mean metallicity of $Z = 0.0005$ (see Section 4.5). The helium-rich ZAHBs appear too bright to explain any significant number of Tucana HB stars.

4. THE STAR FORMATION HISTORY OF TUCANA

The SFH of Tucana was derived, similarly to the other galaxies of the LCID sample, using the two photometry sets, two stellar evolution libraries (BaSTI;[13] Pietrinferni et al. 2004 and Padova/Girardi;[14] Girardi et al. 2000) and three different SFH codes: IAC-pop (Aparicio & Hidalgo 2009), MATCH (Dolphin 2002), and COLE (Skillman et al. 2003). We performed the same kind of analysis already presented for Cetus (Monelli et al. 2010b) and LGS3 (Hidalgo et al. 2010). In particular, we used the three SFH codes together with the DOLPHOT photometry in combination with the Padova stellar evolution library. The IAC-pop solutions were derived using both photometry sets and both libraries.

In the following sections, we summarize the fundamentals of the three SFH methods applied. A comparison of the results is given in Section 4.4, while the Tucana SFH will be discussed in Section 4.5.

4.1. The IAC Method

The IAC method to derive the SFH of resolved stellar systems, based on the IAC-star/IAC-pop/MinnIAC algorithms, has been extensively presented in Aparicio & Hidalgo (2009) and Hidalgo et al. (2010). Due to the similarities between the Tucana and Cetus CMD, we applied the same criteria explained for Cetus

[13] http://www.oa-teramo.inaf.it/BASTI

[14] http://pleiadi.oapd.inaf.it/

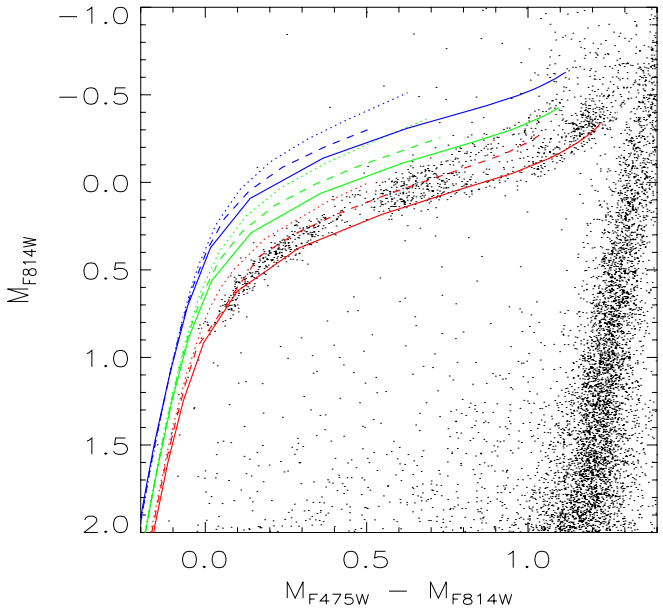

Figure 3. Tucana CMD with superimposed ZAHBs of different metallicities $Z = 0.0001$ (dotted), 0.0003 (dashed), 0.0006 (solid) and $Y = 0.245$ (red), 0.30 (green), 0.35 (blue) are shown. Only the theoretical predictions with normal helium give a good representation of the HB observed in Tucana.

in Monelli et al. (2010b). The reader is referred to that paper for more details and for the discussion of the different choices. In summary, we have adopted the following parameters and functions.

1. *Model functions.* The same synthetic CMDs containing 8×10^6 stars have been used as for Cetus. These were generated using the IAC-star simulator,[15] using:
   (a) the BaSTI and Padova stellar evolution libraries, respectively;
   (b) a constant $\psi(t)$ between 0 and 15 Gyr, and metallicities uniformly distributed in the range $0.0001 < Z < 0.005$;
   (c) a binary fraction[16] $\beta = 0.4$ with mass ratios $q \geqslant 0.5$;
   (d) the initial mass function (IMF) from Kroupa (2001) ($N(m)dm = m^{-\alpha}dm$, where $\alpha = 1.3$, 2.3 for stars with mass smaller and larger than 0.5 $M_\odot$, respectively);
   (e) the set of bolometric corrections from Bedin et al. (2005).

   The observational errors were simulated in the synthetic CMD using the *obsersin* code (Hidalgo et al. 2010).
2. *Simple populations and CMD sampling.* The initial age and metallicity bins defining the simple populations are as follows:
   age: [1.5 2 3 ...11.5 13.5] $\times 10^9$ yr;
   metallicity: [0.1 0.3 0.5 0.7 1 1.5 2] $\times 10^{-3}$.
   The parameterization of the CMD was performed using the same choice of *bundles* and box size presented in Monelli et al. (2010b; see Figure 7). Moreover, the same multiple sampling of both the observed and model CMDs ("*dithering* approach") has been applied, using the MinnIAC code (Aparicio & Hidalgo 2009). Twenty-four solutions with twelve different samplings of the simple populations and two samplings of the positions of the boxes grid each were calculated.
3. *External parameters.* The true distance modulus, $(m - M)_0 = 24.77$,[17] was estimated using the mean magnitude of the RR Lyrae stars (Bernard et al. 2009). We assumed the extinction from Schlegel et al. (1998), $E(B - V) = 0.03$, corresponding to $A_{F475W} = 0.122$ mag and $A_{F814W} = 0.061$ mag. To estimate the effect of the uncertainties affecting the photometry and the transformation to the absolute magnitude plane (calibration, distance, and extinction) and possible model zero points, MinnIAC introduces a grid of magnitude and color shifts to the observed CMD. The values of the mean χ^2 in each node of the grid are analyzed to determine the best solution and the associated shift from the adopted transformation to the absolute plane. In the process, the sets of 24 solutions were calculated 39 times, with different shifts, for a total of 936 solutions. This computationally expensive task was performed using the Condor workload management system[18] (Thain et al. 2005) available at the Instituto de Astrofísica de Canarias. An initial grid with 25 positions was common to the two photometry sets. A second grid with 14 positions is used to refine the search for the best χ^2. In the case of the DAOPHOT photometry, the minimum was confirmed at the position $(\delta_{col}, \delta_{mag}) = (0.0, 0.0)$, $\chi^2_{\nu,min} = 2.63$, while in the case of the DOLPHOT photometry the minimum is located at $(\delta_{col}, \delta_{mag}) = (+0.06, 0.15)$, $\chi^2_{\nu,min} = 2.57$. In the Section 4.5, we describe the details of the two solutions calculated at the $\chi^2_{\nu,min}$ position.

4.2. The Match Method

The principles of the MATCH method of measuring SFHs are presented in Dolphin (2000a) and Dolphin (2002). In this work, to appropriately compare the synthetic and observed CMDs, we converted them into Hess diagrams binning by 0.10 mag in M_{F475W} and 0.05 mag in $M_{F475W} - M_{F814W}$. For consistency, we chose parameters to create synthetic CMDs that closely matched those used in the IAC-pop code presented in this paper:

1. a power-law IMF with $\alpha = 2.3$ from 0.1 to 100 $M_\odot$;
2. a binary fraction $\beta = 0.40$;
3. a distance modulus of 24.77, $A_{F475W} = 0.122$; and
4. the stellar evolution libraries of Marigo et al. (2008), which are the basic Padova/Girardi models with updated AGB evolutionary sequences.

The synthetic CMDs were populated with stars over a time range of $\log t = 6.6$–10.20, with a uniform bin size of 0.1. Furthermore, the program was allowed to solve for the best-fit metallicity per time bin, drawing from a range of [M/H] = −2.3 to 0.1, where M canonically represents all metals. The depth of the photometry used for the SFH was equal to 50% completeness in both M_{F475W} and M_{F814W}.

To quantify the accuracy of the resultant SFH, we tested for both statistical errors and modeling uncertainties. To simulate possible zero-point discrepancies between isochrones and data, we constructed SFHs adopting small offsets in distance and extinction from the best-fit values. The rms scatter between those solutions is a reasonable proxy for uncertainty in the stellar evolution models and/or photometric zero points. Statistical errors were accounted for by solving 50 random realizations

[15] http://iac-star.iac.es
[16] We tested six different values, from $\beta = 0$ to 1. A more detailed discussion can be found in Monelli et al. (2010b).
[17] The value adopted in the SFH derivation, 24.77, is slightly different from the final value of 24.74 ± 0.12 given in (Bernard et al. 2009). However, such a small difference has negligible impact on the derived SFH.
[18] http://www.cs.wisc.edu/condor/

of the best-fit SFH. Final error bars are calculated summing in quadrature the statistical and systematic errors.

4.3. The COLE Method

The third method we applied to measure the SFH of Tucana is a simulated annealing algorithm applied to our DOLPHOT photometry and the Padova/Girardi library. The code is the same as that applied to the galaxies Leo A (Cole et al. 2007) and IC 1613 (Skillman et al. 2003), and details of the method can be found in those references.

In particular, the isochrone tables (Marigo et al. 2008) for each (age and metallicity) pair are shifted by the appropriate distance and reddening values, and transformed into a discrete color–magnitude-density distribution ϱ by convolution with:

1. the IMF from Chabrier (2003);
2. the results of the artificial star tests simulating observational uncertainties and incompleteness; and
3. the binary star frequency and mass ratio distribution from the solar neighborhood, namely 35% of stars are single, 46% are parameterized as "wide" binaries, i.e., the secondary mass is uncorrelated with the primary mass, and is drawn from the same IMF as the primary, and finally 19% of stars are parameterized as "close" binaries, i.e., the probability distribution function of the mass ratio is flat.

The history of the galaxy is then divided into discrete age bins with approximately constant logarithmic spacing. We used 10 time bins ranging from $8.00 \leqslant \log(\mathrm{age/Gyr}) \leqslant 10.13$. Isochrones evenly spaced by 0.2 dex from $-2.3 \leqslant [\mathrm{M/H}] \leqslant -0.9$ were used, considering only scaled-solar abundances but with no further constraints on the age–metallicity relation. The SFH is then modeled as the linear combination of $\psi(t, Z)$ that best matches the data by summing the values of ϱ at each point in the Hess diagram. The CMD was discretized into bins of dimension 0.10×0.20 mag, and it is the density distribution in this Hess diagram that was fit to the models. The error bars are determined by perturbing each component of the best-fit SFH in turn and resolving for a new best fit with the perturbed component held fixed.

4.4. Comparison of the Different Solutions

We verified the consistency of the results obtained with the three methods, observing good agreement as shown in the previous papers. A comparison of the results obtained using different photometry/library/SFH-code combinations is shown in Figure 4, which presents, in the panels (a) and (b), the cumulative mass fraction as a function of time for different combinations of photometry, library, and method. In particular, the panel (a) compares the solutions from the DAOPHOT and the DOLPHOT photometry derived using the BaSTI and the Padova stellar evolution library. Panel (b) shows the solution derived with the three SFH codes, for the DOLPHOT photometry coupled with the Padova library. The two plots disclose a generally very good agreement between the different solutions. Panels (c) and (d) compare the $\psi(t)$ calculated with the three SFH algorithms. It has to be stressed that the three methods use different IMFs, and the comparison of the derived $\psi(t)$ should be done carefully. Therefore, panels (c) and (d) compare the three $\psi(t)$ before and after applying a scaling factor to the MATCH and COLE solutions, in order to take into account the different IMFs. Note the very good agreement in the main features: the position of the main peak at the oldest ages and the subsequent decreasing trend. Both the MATCH and COLE methods give some small residual star formation between 5 and 8 Gyr ago, which is not present in the IAC-pop solution, but still the three solutions are consistent within the error bars.

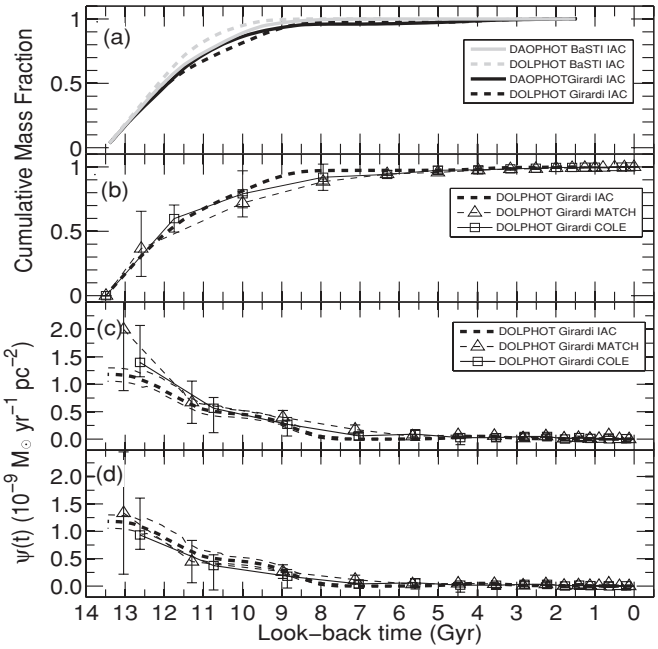

Figure 4. Summary of the results obtained with different techniques to derive the SFH. Top: comparison of the cumulative mass fraction derived from SFH obtained with the MinnIAC/IAC-pop method, using the BaSTI and the Padova library and applied to the DAOPHOT and the DOLPHOT photometry. Middle: same as in the upper panel, but the comparison shows the results from the three different SFH codes, applied to the DOLPHOT photometry in combination with the Padova/Girardi. Bottom: $\psi(t)$ derived for the three solutions presented in the central panel.

4.5. The Tucana SFH

Similarly to the previous works (Monelli et al. 2010b; Hidalgo et al. 2010), we discuss in detail the solution based on the IAC method applied to a model CMD calculated with the BaSTI library and, in particular, the average of the two solutions based on the two sets of photometry.

We present two different representations of both solutions. Figure 5 shows a three-dimensional view of the best solutions, calculated as the running average of the 24 individual solutions at the $\chi^2_{\nu\,\mathrm{min}}$ (Hidalgo et al. 2010). This is a convenient way to have an immediate, general visualization of the stellar content and evolution of a system (Hodge 1989), since it includes the information on the star formation rate as a function of both age and metallicity, and the age and metallicity distributions as projections of the first. Figure 5 shows that the bulk of star formation occurred in Tucana at a very early time and with a limited metallicity range. Only a small percentage of the star formation inferred in the solution occurred at epochs younger than 10 Gyr ago and with metallicity $Z > 0.001$. Another feature that appears in both solutions is a small population of intermediate-age, low-metallicity stars. We interpret this as a population of blue stragglers, because the inferred metallicity is in good agreement with that of the oldest population in Tucana, and it does not follow the general age–metallicity relation of the bulk of stars. The same feature was present in the Cetus SFH presented by Monelli et al. (2010b) and was interpreted similarly. We refer to that reference for further discussion.

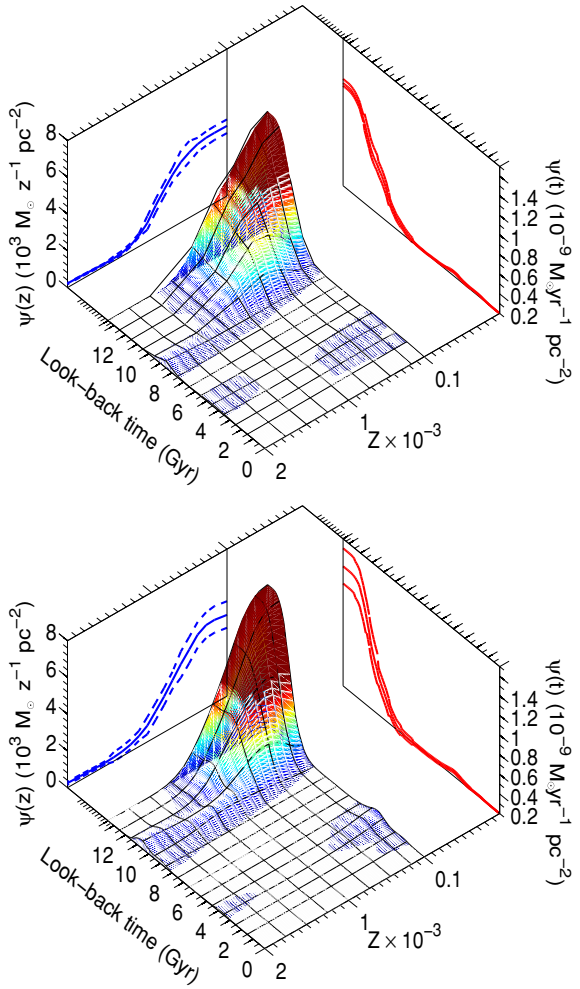

Figure 5. Three-dimensional representation showing the SFH of Tucana, derived with the DAOPHOT (top) and the DOLPHOT (bottom) photometry. Both show the average of 24 solutions calculated at the minimum χ^2 in the δmag − δcol grid.

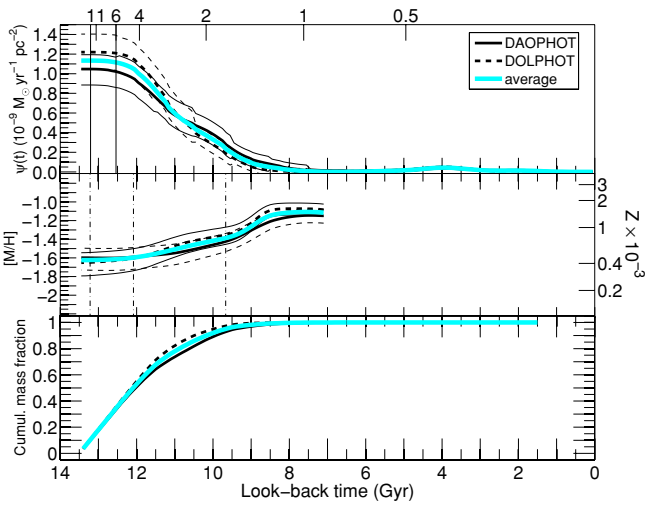

Figure 6. Summary of the Tucana SFH results. The three panels show, from top to bottom, $\psi(t)$, the age–metallicity relation and the cumulative mass fraction. We show the results with the BaSTI library for both the DAOPHOT (dashed line) and the DOLPHOT (continuous) photometry, and the average of the two (thick cyan line). The dashed part of the cyan line representing the average of the two sets of photometry in the middle panel indicates what we believe to be the presence of BSs rather than a low level of intermediate-age and young SF. The thin lines represent the error bars, while the vertical lines in the upper panel mark redshifts $z = 15$ and 6—the epochs corresponding to the reionization. (Bouwens et al. 2007). The dot-dashed lines in the central panel mark the epochs when 10%, 50% and 90% of the stellar mass was formed.

A complementary view is shown in Figure 6, where the star formation rate, the chemical enrichment law, and the cumulative mass fraction are plotted as functions of time. The thick continuous and dashed lines show the DAOPHOT and DOLPHOT solutions, respectively, while the thin lines represent the corresponding error bars. These have been calculated following the prescription given in Hidalgo et al. (2010). Note the good agreement between the solutions based on the two different sets of photometry. Both recover the highest peak as a flat feature at the oldest ages, $t > 12.5$ Gyr ago. The steepness of the decline is marginally different, and both solutions give very similar ages at which the star formation completely stopped in Tucana, around 8–9 Gyr ago. There is also excellent agreement in the small peak detected at ∼4 Gyr ago, related to the BS population. An excellent correspondence is also observed in the derived metallicity laws, represented in the middle panel. A steady increase of [M/H] is observed, from [M/H] ≈ -1.6 at very early times to [M/H] ≈ -1.1 at the end of the star formation activity. After that, the shape of $Z(t)$ is necessarily uncertain given the small number of stars from which it is derived and, therefore, it is not shown in the plot.

Since the small differences in $\psi(t)$ and in the chemical evolution law from the two photometry sets are well within the error bars and because we do not have any reason to prefer one photometry set over the other, it seems reasonable to adopt the average of the two solutions as the Tucana SFH, and the differences between the two as an indication of external errors. The thick cyan lines in Figure 6 represent this average, which we adopt as the final solution for the Tucana SFH.

The upper panel of Figure 6 discloses that no star formation occurred in Tucana in the last ≈8–9 Gyr. This statement can be further quantified by quoting the ages when we estimate that 10%, 50%, and 95% of the stellar mass was formed (≈13.2, 12.1, and 9.7 Gyr ago; these are represented as vertical lines in the middle panel of Figure 6). This result demonstrates that Tucana, like Cetus (Monelli et al. 2010b), is an outlier of the morphology–density relation, because it is a purely old system located at a large distance from both the giant galaxies of the LG.

Figure 7 presents a comparison between the observed DAOPHOT CMD and a best-fit CMD (left and central panels), represented as Hess diagrams. The bundles used to derive the solution have been superimposed on the observed CMD. We find satisfactory agreement in all the main evolutionary phases. As far as the differences in the HB morphology are concerned, it is worth noting that we have not tried to properly reproduce this observational feature. Due to the strong dependence of the HB morphology on the mass-loss processes along the RGB, it is clear that a better agreement between the observational data and the synthetic CMD could be obtained with a better knowledge of the average mass-loss efficiency and its spread. The right panel shows the residual Hess diagram, in units of Poisson error, which supports the good agreement between the observed and the best-fit CMD.

The mean quantities derived (star formation rate, age, and metallicity), together with the integral of the $\psi(t)$, are summarized in Table 1.

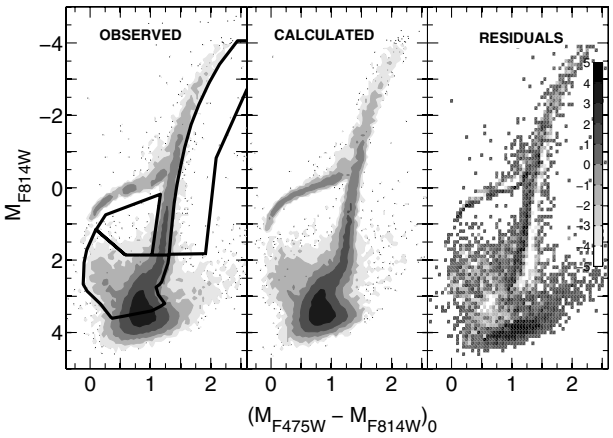

Figure 7. Comparison of the observed (left) and best-fit (center) CMDs. The latter was derived by extracting random stars from the model CMD used to derive the solution, in such a way that each simple population contributes proportionally to the calculated SFR. The black lines in the left panel mark the position of the four bundles adopted to derive the solution. The right panel shows the residual Hess diagram (calculated as observed–model), shown in units of Poisson errors. The figure discloses an overall general agreement between the observed and the best-fit CMDs, particularly in the whole TO region used to calculate the SFH. The discrepancy at the faintest magnitude is due to the limiting magnitude of the model CMD. Note that such a discrepancy does not affect the portion of the CMD included in the bundles. The differences in the HB morphology are expected, since small differences in the adopted mass-loss prescription along the RGB have a big impact on the HB morphology.

Table 1
Integrated Quantities Derived for the Tucana dSph

Quantity	DAOPHOT	DOLPHOT
$\int \psi(t)dt$ (10^6 $M_\odot$)	(2.52 ± 0.02)	(2.62 ± 0.03)
$\langle\psi(t)\rangle$(10^{-7} $M_\odot$ yr^{-1} pc^{-2})	(1.25 ± 0.01)	(1.30 ± 0.01)
$\langle$age$\rangle$(10^{10} yr)	(1.15 ± 0.02)	(1.17 ± 0.01)
$\langle$[Fe/H]$\rangle$(10^{-4} dex)	(5.78 ± 0.83)	(5.63 ± 0.82)

4.6. The Short First Episode of Star Formation in Tucana: Are We Seeing the Effects of Reionization?

The description presented in the previous section corresponds to the SFH of Tucana as derived using the algorithms discussed above. This solution is the convolution of the *actual* Tucana SFH with some smearing produced by the combination of observational errors and the limitations of the SFH recovery method (Aparicio & Hidalgo 2009). These are related in part to intrinsic limitations of the method, such as the small differences in position in the MSTO of old stars of ages within 2–3 Gyr. In the following, we will try to constrain further the features of the *actual*, underlying Tucana SFH through some tests with mock stellar populations.

In particular, to address the question: "did cosmic reionization affect the SFH of Tucana?" we designed a specific test with mock populations. It is generally assumed that the universe was completely reionized by $z \approx 6$, equivalent to a look-back time of ≈12.8 Gyr (Bouwens et al 2007). Therefore, we created three mock stellar populations with constant $\psi(t)$ in the age ranges 13.3 Gyr $< t <$ 12.8 Gyr, 12.8 Gyr $< t <$ 12.3 Gyr, and 12.3 Gyr $<$ 11.8 Gyr ago.[19] We also assumed a

[19] Note that the age derived through the SFH recovery depend on the assumed set of theoretical models. However, it has been shown that the libraries adopted in this work give similar ages (Gallart et al. 2005), and also that the ages derived for the Galactic GCs are in excellent agreement with the age of the universe from the *Wilkinson Microwave Anisotropy Probe* (*WMAP*) experiment (Marín-Franch et al. 2009). This ensures a meaningful comparison between the solution SFH in the same cosmological framework.

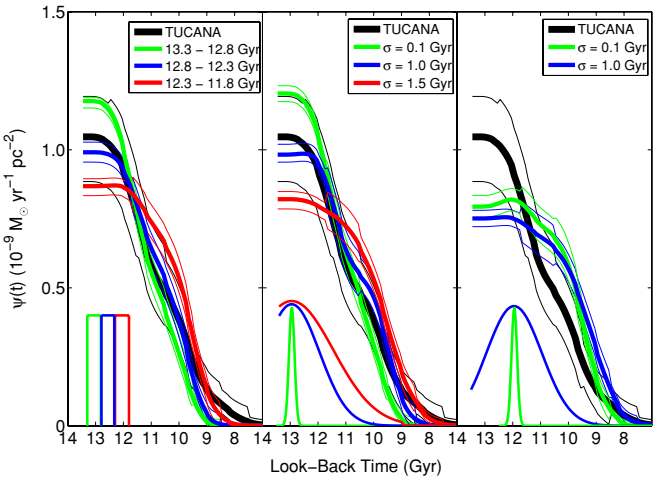

Figure 8. Results of the tests performed recovering the SFH of two mock populations. The left panel compares the Tucana $\psi(t)$ with that of three mock bursts at different ages. The central and right panels compare it with Gaussian profile $\psi(t)$ laws of different σ and mean age. These comparisons disclose that the bulk of the star formation in Tucana occurred between 13.5 and 12 Gyr ago, suggesting that we cannot put firm constraints on the effect of the reionization in this galaxy. Nevertheless, these tests strongly suggest that Tucana could not undergo strong star formation at epochs younger than 12 Gyr ago, although some residual star formation is still compatible with the observed $\psi(t)$.

mean metallicity and a metallicity dispersion similar to what is inferred for Tucana. We simulated the observational errors of the DAOPHOT photometry and recovered the SFH of the mock galaxies with the same prescription as for the real galaxy. In order to minimize the fluctuations associated with the creation of the synthetic CMDs, we repeated each test five times. Figure 8, left panel, shows the mean of the five resulting $\psi(t)$ for each mock population, compared with that of Tucana, shown as a thick black line with the corresponding error bars. Note that the fact of repeating the experiment five times reduces the impact of the Poisson errors, reflected in the smaller error bars of the recovered mock $\psi(t)$. The time extension of the three input bursts is shown schematically at the bottom of the figure. The three recovered functions $\psi(t)$ show similar general behavior, but the main peak is recovered younger and lower, and its width larger, for decreasing age of the input $\psi(t)$. The comparison with the Tucana SFH leads to two main conclusions.

1. Despite the fact that the best agreement at the oldest epoch is obtained with the intermediate-age mock population, the case of the oldest mock population is also compatible, within the error bars, with the SFH observed for Tucana. This suggests that, due to the limited age resolution, we cannot draw definitive conclusions concerning the effect of the reionization on Tucana. In fact, it is equally acceptable that Tucana started forming stars either before or after the universe was completely reionized, more than 12.8 Gyr ago. Moreover, note that if the star formation started before 12.8 Gyr ago, the derived solution may indicate that the star formation extends somewhat toward younger epochs.
2. The youngest mock population is only marginally consistent with the Tucana solution at all ages, strongly suggesting the *bulk* of star formation in this galaxy could not occur at epochs younger than ∼12 Gyr ago. However, it is still possible that some *residual* star formation was active at younger ages.

Note that the mock populations presented in Figure 8 are characterized by a relatively short episode of star formation,

lasting 0.5 Gyr. Nevertheless, the recovered $\psi(t)$ shows a significantly longer duration, comparable to that of Tucana. This suggests that the actual duration of the main star formation event in Tucana was significantly shorter than the calculated one.

To further investigate this point, we simulated more mock populations, with Gaussian input $\psi(t)$ peaked at 13 Gyr ago and with age dispersion $\sigma = 0.1$, 1.0, and 1.5 Gyr. The first two have also been repeated assuming an age peak at 12 Gyr ago. The Gaussian $\psi(t)$ was truncated at the oldest age we are considering, 13.5 Gyr, i.e., no stars older than 13.5 Gyr were allowed in the mock populations. The results are shown in Figure 8, central and right panels. As in the previous test, we repeated each case five times and show the mean recovered $\psi(t)$. The comparison in the central panel shows that the observed peak at the oldest ages is best reproduced by the $\sigma = 1.0$ Gyr Gaussian profile, but it is still compatible with the narrowest one.

On the other hand, the narrowest Gaussian profile does not properly represent the shape of the Tucana $\psi(t)$, suggesting that the first event was somewhat longer than this test case. Similarly, the peak of the widest Gaussian profile appears too low and flat and is not compatible with the observed one. The comparison with the Gaussian $\psi(t)$ peaked at 12 Gyr ago, shown in the right panel, indicates that the bulk of the star formation of these mock populations is too young and is not compatible with the Tucana $\psi(t)$. Note that, in equivalent tests performed for the Cetus dSph in Monelli et al. (2010b), a mock Gaussian population peaked at this age was a good representation of the observed $\psi(t)$. This suggests that, despite the apparent similarities of the calculated SFH of these two galaxies, we are able to disentangle subtle age differences between the two (see Section 5).

We stress that the case of Tucana is possibly the most difficult among the LCID galaxies. The combination of both intrinsic effects (it is the most distant galaxy in our sample and the oldest one) and observational ones (the shortest exposure times due to the South Atlantic Anomaly) contribute to increase the complexity of the problem and the loss of age resolution at the oldest epochs.

4.7. Summary

The SFH of Tucana can be summarized as follows. Tucana experienced a very early and short event of star formation, peaked at ages $t > 12.5$ Gyr ago. We measure a steady decrease in the star formation rate until star formation completely stopped ∼9 Gyr ago. We showed that the measured duration is overestimated and that the actual event is compatible with a Gaussian $\psi(t)$ with σ between $\leqslant$1.0 Gyr. The apparent residual star formation at intermediate ages is interpreted as a population of blue stragglers. The tests performed with mock populations suggest that the epoch of the main episode of star formation is compatible with the end of the reionization era, and that it cannot have occurred later than 12 Gyr ago. This is different from what found for Cetus, where the majority of stars formed at least 1 Gyr later. We will present an in-depth comparison of the two galaxies in the next section.

5. TUCANA AND CETUS

Tucana and Cetus share the noticeable characteristic of being among the most isolated dSph galaxies in the LG. Cetus is located at more than 650 kpc from both the Milky Way and M31. Tucana is even more distant, at 900 kpc from the Milky Way and 1.3 Mpc from M31. The actual position and orbit are crucial to understand interactions that may have occurred in the past. Their receding velocities in respect of the barycenter of the LG (Fraternali et al. 2009; Lewis et al. 2007) suggest that both galaxies may already have experienced at least one passage through the innermost regions of the LG and, in the case of Cetus, that it is close to the apocenter of its orbit.

Therefore, a detailed comparison of their properties can be useful to understand the origin of the differences and similarities in their SFHs.

5.1. Physical Parameters

Table 2 gives a summary of the intrinsic properties of Cetus and Tucana. Cetus is the larger galaxy, both in terms of baryonic mass and physical size. Tucana presents the mass ($1.81\times10^6\ M_\odot$ baryonic mass; Hidalgo et al. 2010) and size (exponential scale length $\alpha \sim 120$ pc) typical of the smallest dSphs in the LG, similar to Sculptor, Leo II, and Ursa Minor. On the other hand, Cetus is similar to the larger nearby dSphs, with mass and size comparable to Carina or And II, with a total baryonic mass of $3.94 \times 10^6\ M_\odot$ and $\alpha \sim 220$ pc. Despite their large distances from both the Milky Way and M31, both Tucana and Cetus are similar to the oldest systems like Draco, Ursa Minor, or Sculptor. However, the velocity dispersion estimated for the two galaxies ($\sigma \sim 17$ km s^{-1}) is significantly higher than the measured dispersion for the nearby dSphs ($\leqslant$10 km s^{-1}). Assuming that the circular velocity of the halo v_c is $v_c = \sqrt{(3)}\sigma$, and the scaling suggested for sub-halos by cosmological simulations (see Kravtsov 2010) and confirmed also by simulations of tidally perturbed satellites with dark matter and stars (Klimentowski et al. 2007), one obtains $v_c \sim 29$ km s^{-1} for the halo of Tucana, which would correspond to a virial mass of $\sim4 \times 10^9\ M_\odot$, higher than that of dSph satellites of the MW (Łokas 2009; Strigari et al. 2010) but comparable to the mass estimated for their progenitors before they were accreted by the Milky Way or M31 halos (Mayer 2010 and see the reviews by Kravtsov 2010). Since Tucana and Cetus have been only weakly affected by tides, the estimated mass should indeed be close to their mass before infall into the primary galaxies. With such a high halo mass, the resulting M/L ratio would be several hundred in solar units. However, both show hints of rotation, and taking this into account would reduce these numbers. Moreover, the faintness of the observed stars, together with the low signal-to-noise ratio (S/N) of the available low-resolution Ca-triplet spectra might also have played a role in overestimating the velocity dispersion. It is nonetheless conceivable that M/L is at least as high as in the most dark-matter-dominated among the classical dSphs, such as Draco, Ursa Minor, and And II.

5.2. The Oldest Stars as a Benchmark for the Reionization Effects

Figure 9 compares the derived properties for Tucana (black line) and Cetus (gray line). The upper panel shows the calculated $\psi(t)$ as the average from the two photometry sets. All the experiments performed to test the IAC-pop code (Aparicio & Hidalgo 2009; Hidalgo et al. 2010; Monelli et al. 2010b), as well as the tests with mock galaxies presented in Section 4.6, support the reliability of the solutions, in relation to the determination of the age of the peak star formation (the typical precision is of the order of 0.5 Gyr, see Monelli et al. 2010b), including at epochs >10 Gyr. Moreover, we stress that we are comparing two SFHs obtained using the same stellar evolution library and the average resulting from the two photometry sets. This minimizes

Table 2
Estimates of the Basic Parameters for the Two dSph Galaxies Tucana and Cetus

Parameter	Tucana	Cetus
D (kpc)	887 ± 50[a]	780 ± 43[a]
$(m-M)_0$	24.74 ± 0.12[a]	24.46 ± 0.12[a]
M_V (mag)	-9.55 ± 0.27[b]	-10.1[c]; -11.3[d]
L_V ($L_\odot$)	5.2×10^5[b]	8.7×10^5[c]; 2.6×10^6[d]
M/L ($M_\odot/L_\odot$)	105^{+95}_{-49}[e]	$\simeq 70$[f]
Total mass ($M_\odot$)	$\simeq 6 \times 10^7$[e]	$\simeq 6 \times 10^7$[f]
Stellar mass ($M_\odot$)	1.81×10^6	3.94×10^6
α ($'$(pc))	$0.48 \pm 0.08(124)$[b]; $0.51(132)$[g]	$1.0 \pm XX(230)$[g]; 1.59 ± 0.05[d]
R_c ($'$(pc))	$0.59(152)$[a]; $0.66 \pm 0.1(170 \pm 25)$[b]	$1.5 \pm 0.1(340)$[c]; $1.3 \pm 0.1(295)$[d]
R_t ($'$(pc))	$3.45(890)$[b]	$4.8 \pm 0.2(1089 \pm 45)$[c]; $32 \pm 6.5(7261 \pm 1475)$[d]
c	0.72[b]	0.5[c]; 1.4[d]
$\mu_{o,V}$ (obs) (mag)	25.05 ± 0.06[b]	25.0[d]
$v_{\rm hel}$ (km s^{-1})	$+194.0 \pm 4.3$[e]	-87 ± 2[f]
$v_{\rm GSR}$ (km s^{-1})	$+98.9$[e]	-25[f]
$v_{\rm LGSR}$ (km s^{-1})	$+73.3$[e]	$+14$[f]
σ (km s^{-1})	$17.4^{-3.1}_{+4.1}$[e]	$17 \pm 2(14 \div 8)$[f]
$v_{\rm rot}$ (km s^{-1})	$\simeq 16$[e]	7.7 ± 1.2[f]
$\langle$age$\rangle$ (Gyr)	11.6 ± 0.1[h]	11.3 ± 0.2[g]
T_{10} (Gyr)	13.2[h]	13.1[g]
T_{50} (Gyr)	12.1[h]	11.6[g]
T_{95} (Gyr)	9.7[h]	9.6[g]

Notes.
[a] Bernard et al. 2009.
[b] Saviane et al. 1996.
[c] Whiting et al. 1999.
[d] McConnachie & Irwin 2006.
[e] Fraternali et al. 2009.
[f] Lewis et al. 2007.
[g] Monelli et al. 2010b.
[h] This work.

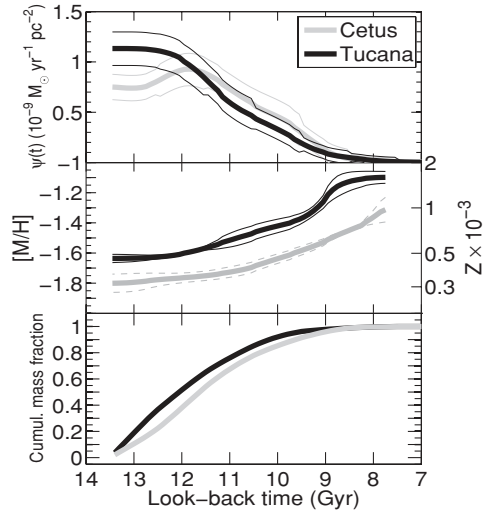

Figure 9. Comparison of the $\psi(t)$ (top), age–metallicity relations (middle), and cumulative mass functions of Tucana and Cetus. The epoch of peak star formation in Tucana is ∼1.0 Gyr earlier than in Cetus.

the possible systematic effects, giving more confidence to the estimate of the *relative* differences between the main SFH features of the two galaxies.

The analysis of the $\psi(t)$ shows that the evolution of the two galaxies was different. Tucana experienced its strongest level of star formation at the earliest epochs, with the initial peak followed by a steady decrease in the star formation rate. On the other hand, the star formation in Cetus (Monelli et al. 2010b) might have started at the same epoch, but with the rate increasing until reaching the main peak ∼1.0 Gyr later. Therefore, there is a strong indication that Cetus formed the majority of its stellar mass significantly after Tucana, as summarized in Table 2 with additional information such as t_{50} and the mean age.

Note that we have observed most of Tucana's body, while in the case of Cetus, the very central region of the galaxy (within $R_{\rm gc} \leqslant 0.5 r_{\rm c}$) was not contained in our ACS data. This may affect somewhat the resulting SFH, in view of the stellar population gradients that are present in these galaxies (which will be discussed in detail in Hidalgo et al. 2010). However, in this study, we found—in agreement with previous works (Gallagher et al. 1998; Harbeck et al. 2001; Monelli et al. 2003; Battaglia et al. 2006; Bernard et al. 2008; Lee et al. 2009)—that the stellar population gradients are in the sense that the population is on average younger in the central part. This implies that the former picture of the differences between the SFH of Tucana and Cetus would unlikely change (or if changing, the differences would only increase) if we could compare with the global SFH of Cetus.

The central panel of Figure 9 shows the comparison of the two age–metallicity relations. The thin lines at either side of each relation indicate the 1σ dispersion of the metallicity distribution at each age; the whole metallicity range at each age is much larger. The run of mean metallicity with age is

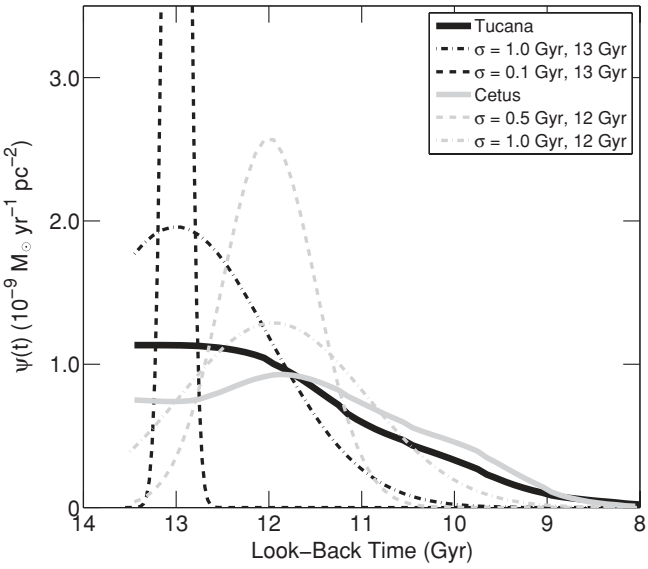

Figure 10. Comparison of the Tucana (left) and Cetus (right) $\psi(t)$ relations with those of Gaussian mock populations giving comparable solutions. The inferred underlying SFHs of Tucana and Cetus support the idea of an earlier and stronger first episode in Tucana.

similar in both galaxies, with the mean metallicity steadily increasing as a function of time. However, Tucana appears more metal-rich than Cetus, at fixed age, in contrast with the metallicity–luminosity relation of dSph galaxies (Grebel et al. 2003), but still consistent with the scatter of that relation. Note that the higher mean metallicity in Tucana does not imply a difference in the metallicity of the most metal-poor populations, which is the same in both galaxies and consistent with $Z = 0.0001$. The higher mean metallicity derived for Tucana may also be connected to the stronger initial event of star formation, which enriched the medium in a short timescale that we are not able to resolve.

The lower panel of Figure 9 compares the cumulative mass fraction as a function of time. Tucana presents a steeper curve, reflecting the discussed stronger initial activity.

As discussed in Hidalgo et al. (2010) and Monelli et al. (2010b), the effect on the derived SFH of our limited age resolution at old ages is mainly to broaden the main features and to artificially extend the limits of the epoch(s) of star formation. The subtle differences between the Tucana and Cetus SFHs may be best visualized in terms of the possible *true, underlying* SFHs that we have discussed for both galaxies, using tests with mock stellar populations. Figure 10 summarizes the comparison of the $\psi(t)$ retrieved for Tucana and Cetus with those of the compatible Gaussian mock populations. Despite being only qualitative, this plot clearly discloses that the star formation in Tucana is expected to have been significantly stronger at the oldest ages than in the case of Cetus and that, since the narrowest events seem to be compatible with the SFH of both galaxies, even the main star formation event may have occurred at almost non-overlapping epochs. Despite the uncertainties possibly affecting the *absolute* age scale and the ambiguity concerning the duration of the main event in Tucana highlighted in Section 4.6 the *relative* difference of 1 Gyr calculated between the inferred peak of the $\psi(t)$ of Tucana and that of Cetus strongly reinforces the conclusions presented in Monelli et al. (2010b), where we argued that the reionization had limited, if any, effects on the star formation of Cetus. This is expected if the halo masses of these dwarfs are $>10^8\ M_\odot$ (Susa & Umemura 2004; Kravtsov 2010), which can be easily argued even if their velocity dispersion is somewhat overestimated. We can rule out the possibility that Cetus experienced the majority of its star formation at epochs earlier than the end of the reionization. This conclusion is solid and is further sustained by the consistent results obtained using different photometry sets, stellar evolution libraries, and SFH codes adopted for the LCID project.

5.3. Morphology of the HB and RR Lyrae Stars Properties

Is it possible to link the resulting SFHs with other independent evidence? A comparison of the Tucana and Cetus CMDs is shown in Figure 2. At a first glance, the striking similarities seen in the shape of the TO region and in the slope and color width of the RGB suggest a similar age range and spread of metal content.

An obvious difference between the two shows up in the morphology of the HB. The HB in Tucana presents a complex morphology, with both the blue and the red side well populated, the red side also presenting a split into two parallel sequences. Cetus presents a redder HB morphology (Sarajedini et al. 2002; Monelli et al. 2010b), but nonetheless the blue side is populated, even if by a many fewer stars. The color of the bluest Cetus HB stars is the same as for Tucana.

Therefore, the color limits of the HB are similar in the two galaxies, at both extremes. If we assume that, in complex systems like these, the prolonged star formation and the associated chemical evolution drive such a color spread, then we can expect that the blue side is populated by the oldest, most metal-poor stars. Therefore, the higher number of stars in this region of the Tucana CMD suggests a much stronger star formation event at older epochs and/or lower metallicities than for Cetus. However, the presence of a few blue HB stars in the latter supports the idea that some amount of very old populations present in both. These considerations are in excellent agreement with the derived SFHs (see Figures 8 and 10).

The same scenario is also nicely supported by the properties of the RR Lyrae stars. Bernard et al. (2008) showed the presence of two sub-populations of RR Lyrae stars in Tucana, characterized by different mean luminosities, different mean periods, different slopes of the period–amplitude relation, and different radial distributions. The interpretation of this evidence is that the two sub-populations have different properties in terms of age and/or metallicity. Note that the fainter sample, presumably the younger and more metal-rich, is also the more centrally concentrated. A similar dichotomy was not detected in Cetus, where the sample of RR Lyrae presents homogeneous properties.

The presence of two sub-populations of old stars in Tucana, supported by both the split in the red HB and the properties of the RR Lyrae stars, implies that the first generation is numerous enough to show up clearly and that Tucana was able to produce a second generation of stars with distinct chemical properties due to the self-enrichment from the previous event. The time resolution achievable with the present data is not enough to distinguish an episodic from a continuous $\psi(t)$. Nevertheless, the chemical enrichment seems to have occurred on very short timescale. The fact that the mean metallicity is relatively high even at the oldest epochs (see Figure 9, central panel) indicates that the enrichment occurred very early. Therefore, the derived SFH, dominated by a single event, is still compatible with two populations of old stars identified through other evidence.

5.4. The RGB Bump

The RGB bump is a well-defined feature in the CMD of both galaxies (see Figure 2 and Monelli et al. 2010a). In particular, Tucana presents two bumps, a bluer and brighter one, well separated from a second which is redder and fainter. Cetus only shows one well-populated bump, located on the red side of the RGB. In Monelli et al. (2010a), we discussed how these observed features can be interpreted using the SFHs of the two galaxies, and we put constraints on the age and the metallicity of the populations which produce them. More metal-poor stars ($Z < 0.0005$) produce the brighter bump in Tucana, while the fainter, which is also more populated, consists of slightly more metal-rich stars ($0.0005 < Z < 0.001$). In Cetus, the dominant population ($0.0003 < Z < 0.0006$) produces the single bump. The RGB bumps, therefore, also reflect the previously discussed differences in the Tucana and Cetus SFHs, with an older, more metal-poor population in Tucana numerous enough to show in a separate RGB bump in the blue part of the RGB.

5.5. Summary

All these pieces of information give a coherent picture of the evolution of Cetus and Tucana and of the origin of the subtle differences we have detected. The SFH of Tucana is compatible with a very old and brief event. The presence of two sub-populations of old stars in Tucana, supported by both the split in the red HB and the properties of the RR Lyrae stars and the double RGB bump, implies that Tucana was able to produce a second generation of stars with distinct chemical properties due to self-enrichment from the first stars. The important fraction of very metal-poor stars in Tucana indicates a high efficiency of star formation at the earliest stages. We cannot distinguish, with the present data, between two discrete events or a continuous process.

On the other hand, Cetus started forming stars most likely at the same epoch, as indicated by the bluest HB stars. However, Cetus seems to have had a more gradual evolution, reaching its peak star formation 1 Gyr after Tucana, and producing a dominant population with more homogeneous metallicity. It contains a minority of old, metal-poor stars, like the oldest stars in Tucana, and a majority of slightly younger stars (and possibly somewhat metal enriched with respect to the oldest). The different mean metallicities of Cetus and Tucana can be possibly explained by the intense initial episode of star formation that Tucana experienced at older epochs, that enriched the medium causing the higher metallicity of the subsequent generation of stars.

According to the most widely accepted cosmological framework, the age of the universe is ∼13.7 Gyr, and the best estimate of the reionization epoch is at $z \sim 10.9 \pm 1.4$ (Komatsu et al. 2009). Therefore, the most important conclusion we can draw from the comparison of the SFH of Cetus and Tucana is that the vast majority of the stars in Cetus were born after the end of the reionization, currently assumed at $z \sim 6$. This confirms that the reionization cannot have been the dominant mechanism causing the end of star formation in Cetus (Monelli et al. 2010b). On the other hand, the timescale of the star formation in Tucana suggests that the reionization may have played an important role in this galaxy.

6. DISCUSSION

The SFH of the Tucana isolated dSph galaxy presented in this paper shows that the star formation was very active at very early epochs (>12.5 Gyr ago) and over a short timescale (compatible with a Gaussian $\psi(t)$ with σ in the range $t \leqslant 1.0$ Gyr). The tests we performed with mock galaxies show that the present data do not allow enough time resolution to firmly correlate the epoch of the reionization with the end of the star formation in Tucana. The comparison with Cetus discloses that the latter undoubtedly experienced delayed activity, as compared with Tucana, and the vast majority of its stars were formed significantly later than the end of the reionization era. This would be compatible with the higher mass of Cetus and with the fact that lower mass systems are expected to form earlier (Kravtsov 2010). However, it is particularly intriguing that LGS3 is found to be less massive than Tucana, but nevertheless it formed 80% of its stars well after the end of the reionization, with a peak star formation at the same age as in Cetus (Hidalgo et al. 2010).

Given this, if we assume that the end of the star formation was not predominantly induced by the reionization, what was the cause? In the following, we explore possible alternative mechanisms, both internal and external, that might have affected the evolution of Tucana.

6.1. The Effect of SN Explosions

We will explore here the possibility that the star formation in Tucana was stopped by the removal of the gas by purely internal processes, such as the explosion of SNe. Given the adopted IMF (assumed from Kroupa 2001), coupled with the accurate estimate of the total mass transformed into stars in the galaxy (obtained as the integral of the star formation in the main event, reported in Table 2), it is possible to calculate the expected total number of type II SNe originating from the explosion of massive stars. At the metallicity typical of the Tucana population, we can assume that SNe II originate from stars with masses larger than $\approx 6.5\ M_{\odot}$. Integrating the IMF, and assuming $3.2 \times 10^6\ M_{\odot}$ to be the mass of stars formed as derived from the SFH, we estimate a total number of ∼54,300 SNe II events. This total number does not depend on the duration of the burst, but the number of SNe per unit time increases for decreasing duration of the star formation event. For the two cases examined in Section 4.6, we can assume a duration equal to the FWHM of the input Gaussian: 0.235 Gyr and 1.67 Gyr for the $\sigma = 0.1$ and 1.0 Gyr cases. Note that, in the latter case, the assumed duration is smaller than the theoretical value of 2.35 Gyr because we consider only stars younger than 13.5 Gyr. Assuming that each SN releases 10^{51}erg, this implies a total luminosity of 7.33×10^{39} erg s^{-1} and 1.03×10^{39} erg s^{-1}, for the 0.1 and 1.0 Gyr events, respectively.[20] If we compare these numbers with the model proposed by Mac Low & Ferrara (1999, see their Figure 1), we can see that in both cases Tucana is in the so-called blowout regime, meaning that part of the gas must be lost due to the wind produced by SNe. This gives a general indication that gas loss and especially the loss of metals directly connected with the SN winds are efficient mechanisms in small systems like Tucana (Mac Low & Ferrara 1999; Ferrara & Tolstoy 2000; Sawala et al. 2010).

However, we have shown strong evidence that two stellar populations with different properties formed in Tucana on a short timescale, and that the younger population was enriched

[20] Note that this can be considered a conservative upper limit, since the total number of expected SN critically depends on the minimum stellar mass assumed to produce an SN event. This, in turn, strongly depends on the overshooting and the mass loss experienced by the stars during their evolution: the effect of mass loss is to increase the mass of stars ending as an SN, therefore decreasing the number of events.

by the yield of the previous one. This has two important implications: (1) Tucana was able to retain a sizable fraction of its gas after a first episode and (2) the time between the two episodes of star formation was long enough to enrich and mix the medium. Given these two results, it is possible to estimate both the minimum timescale required to start enriching the medium and amount of yield that has been produced by the first generation and recycled by the second one, and thus to estimate the amount of metals lost in an independent way.

In the case of SNe II, the typical timescale is extremely short, of the order of few Myr. In the case of SNe Ia, this is related to the evolution of intermediate-mass stars in binary systems, which ends up with a degenerate CO core of mass insufficient for quiet ignition of the C burning. The mass limit of the star that produces a degenerate CO core has been shown to depend on the metallicity of the star (Cassisi & Castellani 1993). For the assumed peak metallicity of the oldest population, the star with largest initial mass capable of producing a degenerate CO core is expected to be $\approx 6.5\,M_{\odot}$ star. The evolutionary time of such stars fixes a minimum timescale for the creation of SNe Ia of $\sim$60 Myr. This suggests that, even in the scenario of the shortest Gaussian profile burst, SNe Ia were capable of contributing to the enrichment of the interstellar medium of Tucana.

Second, it is possible to estimate the number of SNe required to produce the iron that enriched the more metal-rich population in Tucana. The morphology of the HB suggests that the two populations of old stars are compatible with mean metallicities $Z = 0.0002 \pm 0.0001$ and $Z = 0.0006 \pm 0.0002$, according to the comparison with theoretical ZAHBs and the SFH results. Based on the star counts on the HB, where the two populations can be more easily split, we find that each of the two episodes formed $\sim$50% of the stars. Assuming the above metallicities and considering the total mass of stars formed, we can calculate the total mass of the metals contained in the younger population. In particular, assuming that each episode formed $1.6 \times 10^6\,M_{\odot}$, it turns out that $640\,M_{\odot}$ of heavy elements are recycled by the second generation. Assuming the solar mixture from Grevesse & Noels (1993), the amount of iron expected is $\approx 46\,M_{\odot}$. If we assume that only SNe II are involved, using the iron mass production rate from Nomoto et al. (1997b), we estimate that $\sim$300 SNe II are enough to produce this amount of iron. This estimate was derived assuming the iron mass production of a $13\,M_{\odot}$ star. This value might change by a factor of 2–3 with different assumptions. We can now compare this number with the total expected number of SNe II derived before. If we take into account that stars more massive than $\sim 25\,M_{\odot}$ do not enrich the medium, because they end up as neutron stars or black holes, we derive that, from a total of $\sim$23,540 SNe II releasing iron during the first star formation event, only $\approx$1.3% of the iron mass is recycled, while the vast majority is lost, in agreement with the model by Mac Low & Ferrara (1999). On the other extreme, since SNe Ia are more efficient producers of iron (Nomoto et al. 1997a), we estimate that only $\sim$70 SNe Ia are required to produce the iron present in the younger population and that therefore an even larger fraction of gas is lost.

6.2. The Effect of the Environment

The SFH presented in this paper proves that Tucana, like Cetus, is an outlier in the morphology–density relation. Despite its large distance from both the Milky Way and M31, Tucana is a purely old galaxy, similar to the oldest satellites of the Milky Way like Draco, Ursa Minor, or Sculptor, with which it seems to share also a very high M/L. This poses interesting questions on the effectiveness of the environment in shaping the SFH. Why is a galaxy that spent most of its life in isolation so similar to galaxies of similar mass which are close satellites? The idea that close encounters with giant galaxies can influence the evolution of dwarf galaxies is a well-established prediction of models (Mayer et al. 2001; Mayer 2010; Łokas et al. 2010). However, at least 2–3 orbits on relatively small pericenters (<50 kpc) are typically required to completely transform an initially gas-rich disky-like dwarf into a dSph, leaving a nearly isotropic stellar component supported by stellar velocity dispersion rather than rotation (Klimentowski et al. 2009; Łokas 2009). A single passage on a relatively wide orbit (for an orbit with a 1:10 ratio between apocenter and pericenter, which is slightly larger than the mean but still common for sub-halos in cosmological LCDM simulations—see, e.g., Diemand et al. 2007 and Klimentowski et al. 2010, the pericenter distance of Tucana must have been at $R > 50$ kpc) would produce a remnant retaining significant rotation and deviations from sphericity (Kazantzidis et al. 2010). While the residual rotation in Tucana argues in favor of the latter possibility, its structure and kinematics are not firm enough yet to allow drawing conclusions of this sort.

However, based on actual knowledge of the orbit of Tucana, it is concluded that it may have experienced at most one close encounter with an LG giant galaxy. In fact, the velocity of Tucana with respect to the barycenter of the LG, $v_{\rm LGSR} = +73.3$ km s^{-1} (Fraternali et al. 2009), suggests that a close encounter in the densest LG regions was possible, and in particular the velocity with respect to the Milky Way, $v_{\rm GSR} = +98.9$ km s^{-1}, is compatible with an encounter that occurred at $t_{\rm enc} \leqslant 10$ Gyr ago (Fraternali et al. 2009). This is somewhat later than the main star formation epoch identified in this paper, which appears to have ended between 12.5 and 11.5 Gyr ago, but two events could have been nearly simultaneous, given the large uncertainties. A single passage at a distance of tens of kpc could be enough to strip most of the interstellar medium of the galaxy by ram pressure (Mayer et al. 2007), provided that the coronal gas density around the proto-Milky Way was as high as suggested by observational constraints on its present state ($\sim 10^{-4}$ atoms cm^{-3}). Heating by SN feedback and by the cosmic ionizing background, which remained high down to $z \approx 2$, would have rendered the gas more diffuse and pressure-supported, facilitating stripping by the combined action of ram pressure and tides (Mayer et al. 2006; Mayer 2010). However, it should be taken into account that at such early epochs the size of the Milky Way and M31 was significantly smaller, so the effects of a close encounter might not have been as significant. Also, the structure of the coronal gas at such high redshift, when galaxies are undergoing rapid gas accretion via cold flows (Dekel et al. 2009; Agertz et al. 2009), is unclear; while in principle gas densities around the primary could be even higher than at present as the filamentary flows are made of cold relatively dense gas, the halo might not be filled with gas everywhere as in a smooth corona.

Moreover, if it turns out that Tucana has little or no residual rotation, a complete transformation via tidal perturbations after only one pericenter passage would require quite specific conditions, based on gravitational resonances occurring during the interaction (D'Onghia et al. 2009). Another possibility is that Tucana was pushed to its highly eccentric orbit as a result of a three-body interaction (Sales et al. 2007), and thus could have had more than one close encounter with one of the primary galaxies. Finally, in cosmological simulations, a few sub-halos undergo interactions and mergers with other sub-halos before being accreted by the primaries (Kravtsov et al. 2004;

Klimentowski et al. 2010), which could also produce a dSph out of two interacting small disky dwarfs well outside the virial radius of the primary.

On the other hand, the evidence that the properties of nearby and isolated dSphs present important similarities might indicate that interactions are not *the* dominant mechanism shaping these galaxies. For example, the SN explosions from the first generation of stars contributed to the turbulence of the gas. This would have made the gas easier to strip (Murakami & Babul 1999) via ram pressure. Therefore, internal (SN), external (interactions, gas stripping, and ram pressure), or global (reionization) mechanisms can be at play, and the combination of these might have shaped the morphology of some dSphs even before accretion into the satellite system of a large galaxy (Sawala et al. 2010). An analysis based on homogeneous SFHs derived for both the Milky Way and M31 satellite galaxies, together with reliable knowledge of their orbits, would be needed for a meaningful comparison of their properties with those of Tucana and Cetus, in order to gain some insight into the role of the environment in the evolution of small systems.

6.3. Tucana as a High-z Galaxy

The range of estimated burst duration for Tucana ($\sigma \leqslant 1.0$ Gyr) allows us to infer the corresponding actual peak intensity of the initial burst: assuming $\sigma \geqslant 0.1$ Gyr, this ranges from 0.3 to $1.3 \times 10^{-8}\, M_{\odot}\ \mathrm{pc}^{-2}\ \mathrm{yr}^{-1}$. Note that this is the average value, as calculated over the whole area covered, from the center to $\sim$3 core radii. Preliminary analysis of the $\psi(t)$ as a function of radius (Hidalgo et al. 2010) shows that the star formation rate in the innermost regions is $\approx$4 times higher than the average value. This means that the SFR of Tucana, during the first stages of its evolution, was comparable to that observed for present day Blue Compact Dwarf galaxies (see Annibali et al. 2003 and references therein).

Despite the fact that we cannot put a stringent constraint on the end of the star formation in Tucana, a solid result of our analysis is that Tucana was efficiently forming stars at epochs at least as old as $z \sim 7$. In various recent works (Bouwens et al. 2010a, 2010b; González et al. 2010; Labbé et al. 2010; Oesch et al. 2010), galaxies at similar redshift have been identified and characterized for the first time. However, all the galaxies so far detected have masses and luminosity at least two orders of magnitude larger than Tucana (González et al. 2010).

7. SUMMARY AND CONCLUSIONS

Deep *HST*/ACS data have allowed us to derive the lifetime SFH of the Tucana dwarf galaxy, one of the most isolated dSphs in the LG. We have shown that Tucana experienced a strong event of star formation at the oldest possible age, >12.5 Gyr ago. After the first initial peak, the measured intensity of the star formation steadily decreased until stopping $\approx$9 Gyr ago. The tests we performed with mock stellar populations disclose the broadening effect of the observational errors. We find that the actual underlying SFH is compatible with an episode of short duration, in the range $\sigma \leqslant 1.0$ Gyr, if we assume a Gaussian profile $\psi(t)$ peaked 13 Gyr ago. Our attempt to put firm constraints on the age limits of the main event of star formation are hampered by the limited time resolution, and thus we are not able to clearly answer the question of whether the reionization was decisive in ending Tucana's star formation activity.

We explored alternative mechanisms (both external and internal) that may have shaped Tucana's evolution. On the one hand, current measurements of its radial velocity do not rule out the possibility that Tucana may have traversed the inner regions of the LG once. Therefore, a morphological transformation linked to a close interaction with a larger LG member at a time consistent with the end of its star formation cannot be ruled out. On the other hand, we explored the possibility that the feedback from SN explosions might have been responsible for the gas loss. We used two different arguments to conclude that gas loss connected to SN events must indeed have been very important in Tucana's early evolution: first, comparison of the total amount of energy released by the SNe expected in the early evolution of Tucana with the model by Mac Low & Ferrara (1999) shows that Tucana could be in the blowout region. Second, investigating the chemical difference between two main sub-populations of distinct metallicity present in Tucana, we found evidence that the vast majority of the metals produced by the SNe must have been lost by Tucana to the intergalactic medium.

We devoted a particular effort to compare the properties of Tucana and Cetus, the two isolated dSphs analyzed consistently in the LCID project, that also share the important characteristic of being the most isolated dSphs in the LG. Both are (at first approximation) as old as the oldest Milky Way satellites, such as Draco, UMi, or Sculptor, with no traces of star formation younger than $\simeq$9 Gyr. The fact that they do not follow the morphology–density relation that has been observed in Milky Way dSph satellites poses interesting questions concerning the effectiveness of the environment in shaping the SFHs of dwarf galaxies. This gives some support to models such as the one recently published by Sawala et al. (2010) in which internal mechanisms such as SNe, enhanced by the effects of cosmic reionization, are able to reproduce the main characteristics of dSph galaxies without having to invoke strong environmental effects. Still, new clues will come from a better understanding of the structure and kinematics of the stellar component of Tucana and by comparing such properties in detail with those of the classical dSph satellites that were clearly affected by the environment.

Despite the obvious similarities in the CMDs and SFHs of Cetus and Tucana, we also demonstrated important differences in their early evolution. We have shown that the formation time of the bulk of the stellar populations in Cetus is clearly delayed compared to Tucana. This clearly appears in the derived SFHs, and other independent indicators support the same conclusion: the morphology of the HB, the properties of the RR Lyrae variable stars (Bernard et al. 2008, 2009), and the characteristics of the RGB bump (Monelli et al. 2010a). The most important conclusion we can draw from this comparison is that it strongly reinforces the conclusions of Monelli et al. (2010b), in particular that the vast majority of the stars in Cetus were formed well after the end of the reionization epoch, therefore suggesting that the end of the star formation in Cetus was not predominantly caused by it. This has important implications for state-of-the-art models on the effects of reionization in the early SFH of dwarf galaxies.

Support for this work was provided by NASA through grant GO-10515 from the Space Telescope Science Institute, which is operated by AURA, Inc., under NASA contract NAS5-26555, the IAC (grant 310394), and the Education and Science Ministry of Spain (grants AYA2004-06343 and AYA2007-3E3507). This research has made use of NASA's Astrophysics Data System Bibliographic Services and the NASA/IPAC Extragalactic

Database (NED), which is operated by the Jet Propulsion Laboratory, California Institute of Technology, under contract with the National Aeronautics and Space Administration.

Facility: HST (ACS)

REFERENCES

Agertz, O., Teyssier, R., & Moore, B. 2009, MNRAS, 397, L64
Annibali, F., Greggio, L., Tosi, M., Aloisi, A., & Leitherer, C. 2003, AJ, 126, 2752
Aparicio, A., & Gallart, C. 2004, AJ, 128, 1465
Aparicio, A., & Hidalgo, S. L. 2009, AJ, 138, 558
Babul, A., & Rees, M. J. 1992, MNRAS, 255, 346
Barkana, R., & Loeb, A. 1999, ApJ, 523, 54
Battaglia, G., et al. 2006, A&A, 459, 423
Battinelli, P., & Demers, S. 2000, AJ, 120, 1801
Bedin, L., Cassisi, S., Castelli, F., Piotto, G., Anderson, J., Salaris, M., Momany, Y., & Pietrinferni, A. 2005, MNRAS, 357, 1038
Bernard, E., et al. 2008, ApJ, 678, L21
Bernard, E., et al. 2009, ApJ, 699, 1742
Bouwens, R. J., Illingworth, G. D., Franx, M., & Ford, H. 2007, ApJ, 670, 928
Bouwens, R. J., et al. 2010a, ApJ, 709, L133
Bouwens, R. J., et al. 2010b, arXiv:1003.1706
Bullock, J. S., Kravtsov, A. V., & Weinberg, D. H. 2000, ApJ, 539, 517
Caloi, V., & D'Antona, F. 2005, A&A, 435, 987
Carraro, G., Chiosi, C., Girardi, L., & Lia, C. 2001, MNRAS, 327, 69
Cassisi, S., & Castellani, V. 1993, ApJS, 88, 509
Castellani, M., Marconi, G., & Buonanno, R. 1996, A&A, 310, 715
Chabrier, G. 2003, PASP, 115, 763
Chiba, M., & Nath, B. B. 1994, ApJ, 436, 618
Cole, A., et al. 2007, ApJ, 659, 17
Corwin, H. G., Jr., de Vaucouleurs, G., & de Vaucouleurs, A. 1985, Southern Galaxy Catalogue (Austin, TX: Univ. Texas Press)
Da Costa, G. S., & Armandroff, T. E. 1990, AJ, 100, 162
Dekel, A., Sari, R., & Ceverino, D. 2009, ApJ, 703, 785
Diemand, J., Kuhlen, M., & Madau, P. 2007, ApJ, 667, 859
Dolphin, A. E. 2000a, MNRAS, 313, 281
Dolphin, A. E. 2000b, PASP, 112, 1383
Dolphin, A. E. 2002, MNRAS, 332, 91
D'Onghia, E., Besla, G., Cox, T. J., & Hernquist, L. 2009, Nature, 460, 605
Efstathiou, G. 1992, MNRAS, 256, 43
Ferrara, A., & Tolstoy, E. 2000, MNRAS, 313, 291
Ford, H. C., et al. 1998, Proc. SPIE, 3356, 234
Fraternali, F., Tolstoy, E., Irwin, M. J., & Cole, A. A. 2009, A&A, 499, 121
Gallagher, J. S., Tolstoy, E., Dohm-Palmer, R. C., Skillman, E. D., Cole, A. A., Hoessel, J. G., Saha, A., & Mateo, M. 1998, AJ, 115, 1869
Gallart, C., Aparicio, A., & Vilchez, J. M. 1996, AJ, 112, 1928
Gallart, C., Zoccali, M., & Aparicio, A. 2005, ARA&A, 43, 387
Girardi, L., Bressan, A., Bertelli, G., & Chiosi, C. 2000, A&AS, 141, 371
Gnedin, N. Y., & Kravtsov, A. V. 2006, ApJ, 645, 1054
González, V., Labbé, I., Bouwens, R. J., Illingworth, G., Franx, M., Kriek, M., & Brammer, G. B. 2010, ApJ, 713, 115
Grebel, E. K., Gallagher, J. S., III, & Harbeck, D. 2003, AJ, 125, 1926
Grevesse, N., & Noels, A. 1993, Phys. Scr., T47, 133
Harbeck, D., et al. 2001, AJ, 122, 3092
Hidalgo, S., et al. 2010, ApJ, submitted
Hodge, P. 1989, ARA&A, 27, 139
Holtzman, J. A., Afonso, C., & Dolphin, A. 2006, ApJS, 166, 534
Ikeuchi, S. 1986, Ap&SS, 118, 509
Kazantzidis, S., Abadi, M. G., & Navarro, J. F. 2010, ApJ, 720, L62
Kepner, J. V., Babul, A., & Spergel, D. N. 1997, ApJ, 487, 61
Klimentowski, J., Łokas, E. L., Kazantzidis, S., Mayer, L., & Mamon, G. A. 2009, MNRAS, 397, 2015
Klimentowski, J., Łokas, E. L., Kazantzidis, S., Prada, F., Mayer, L., & Mamon, G. A. 2007, MNRAS, 378, 353
Klimentowski, J., Łokas, E. L., Knebe, A., Gottlöber, S., Martinez-Vaquero, L. A., Yepes, G., & Hoffman, Y. 2010, MNRAS, 402, 1899
Komatsu, E., et al. 2009, ApJS, 180, 330
Kravtsov, A. 2010, Adv. Astron., 2010, 281913
Kravtsov, A. V., Berlind, A. A., Wechsler, R. H., Klypin, A. A., Gottlöber, S., Allgood, B., & Primack, J. R. 2004, ApJ, 609, 35
Kroupa, P. 2001, MNRAS, 322, 231
Labbé, I., et al. 2010, ApJ, 708, L26
Lavery, R. J. 1990, IAU Circ., 5139, 2
Lavery, R. J., & Mighell, K. J. 1992, AJ, 103, 81
Lee, M. G., Yuk, I.-S., Park, H. S., Harris, J., & Zaritsky, D. 2009, ApJ, 703, 692
Lewis, G. F., Ibata, R. A., Chapman, S. C., McConnachie, A., Irwin, M. J., Tolstoy, E., & Tanvir, N. R. 2007, MNRAS, 375, 1364
Łokas, E. L. 2009, MNRAS, 394, L102
Lokas, E. L., Kazantzidis, S., Klimentowski, J., Mayer, L., & Callegari, S. 2010, ApJ, 708, 1032
Mac Low, M.-M., & Ferrara, A. 1999, ApJ, 513, 142
Marigo, P., Girardi, L., Bressan, A., Groenewegen, M. A. T., Silva, L., & Granato, G. L. 2008, A&A, 482, 883
Marín-Franch, A., et al. 2009, ApJ, 694, 1498
Mateo, M. L. 1998, ARA&A, 36, 435
Mayer, L. 2010, Adv. Astron., 2010, 278434
Mayer, L., Governato, F., Colpi, M., Moore, B., Quinn, T., Wadsley, J., Stadel, J., & Lake, G. 2001, ApJ, 559, 754
Mayer, L., Kazantzidis, S., Mastropietro, C., & Wadsley, J. 2007, Nature, 445, 738
Mayer, L., Mastropietro, C., Wadsley, J., Stadel, J., & Moore, B. 2006, MNRAS, 369, 1021
McConnachie, A. W., & Irwin, M. J. 2006, MNRAS, 365, 1263
Milone, A. P., et al. 2008, ApJ, 673, 241
Milone, A. P., et al. 2010, ApJ, 709, 1183
Monelli, M., Cassisi, S., Bernard, E. J., Hidalgo, S. L., Aparicio, A., Gallart, C., & Skillman, E. D. 2010a, ApJ, 718, 707
Monelli, M., et al. 2003, AJ, 126, 218
Monelli, M., et al. 2010b, ApJ, 720, 1225
Murakami, I., & Babul, A. 1999, MNRAS, 309, 161
Nomoto, K., Hashimoto, M., Tsujimoto, T., Thielemann, F.-K., Kishimoto, N., Kubo, Y., & Nakasato, N. 1997b, Nucl. Phys. A, 616, 79
Nomoto, K., Iwamoto, K., Nakasato, N., Thielemann, F.-K., Brachwitz, F., Tsujimoto, T., Kubo, Y., & Kishimoto, N. 1997a, Nucl. Phys. A, 621, 467
Oesch, P. A., et al. 2010, ApJ, 709, L21
Okamoto, T., & Frenk, C. S. 2009, MNRAS, 399, L174
Pietrinferni, A., Cassisi, S., Salaris, M., & Castelli, F. 2004, ApJ, 612, 168
Piotto, G., et al. 2005, ApJ, 621, 777
Quinn, T., Katz, N., & Efstathiou, G. 1996, MNRAS, 278, L49
Rees, M. J. 1986, MNRAS, 218, 25P
Ricotti, M., & Gnedin, N. Y. 2005, ApJ, 629, 259
Sales, L. V., Navarro, J. F., Abadi, M. G., & Steinmetz, M. 2007, MNRAS, 379, 1475
Sarajedini, A., et al. 2002, ApJ, 567, 915
Saviane, I., Held, E. V., & Piotto, G. 1996, A&A, 315, 40
Sawala, T., Scannapieco, C., Maio, U., & White, S. 2010, MNRAS, 402, 1599
Schlegel, D. J., Finkbeiner, D. P., & Davis, M. 1998, ApJ, 500, 525
Sirianni, M., et al. 2005, PASP, 117, 1049
Skillman, E. D., Tolstoy, E., Cole, A. A., Dolphin, A. E., Saha, A., Gallagher, J. S., Dohm-Palmer, R. C., & Mateo, M. 2003, ApJ, 596, 253
Stetson, P. B. 1994, PASP, 106, 250
Stinson, G. S., Dalcanton, J. J., Quinn, T., Kaufmann, T., & Wadsley, J. 2007, ApJ, 667, 170
Strigari, L. E., Frenk, C. S., & White, S. D. M. 2010, MNRAS, 1311
Susa, H., & Umemura, M. 2004, ApJ, 610, L5
Tassis, K., Abel, T., Bryan, G. L., & Norman, M. L. 2003, ApJ, 587, 13
Thain, D., Tannebaum, T., & Livny, M. 2005, Concurrency—Practice and Experience, 17, 323
Thoul, A. A., & Weinberg, D. H. 1996, ApJ, 465, 608
Valcke, S., de Rijcke, S., & Dejonghe, H. 2008, MNRAS, 389, 1111
van den Bergh, S. 1999, AJ, 117, 2211
Whiting, A. B., Hau, G. K. T., & Irwin, M. 1999, AJ, 118, 2767